Stem Cell Reports
Article

ISSCR

OPEN ACCESS

Adult Mouse Liver Contains Two Distinct Populations of Cholangiocytes

Bin Li,[1] Craig Dorrell,[1] Pamela S. Canaday,[1] Carl Pelz,[2] Annelise Haft,[1] Milton Finegold,[4] and Markus Grompe[1,2,3,*]

[1]Oregon Stem Cell Center
[2]Papé Family Pediatric Research Institute
[3]Department of Pediatrics
Oregon Health and Science University, Portland, OR 97239, USA
[4]Department of Pathology, Texas Children's Hospital, Houston, TX 77030, USA
*Correspondence: grompem@ohsu.edu
http://dx.doi.org/10.1016/j.stemcr.2017.06.003

SUMMARY

The biliary system plays an important role in several acquired and genetic disorders of the liver. We have previously shown that biliary duct epithelium contains cells giving rise to proliferative Lgr5$^+$ organoids *in vitro*. However, it remained unknown whether all biliary cells or only a specific subset had this clonogenic activity. The cell surface protease ST14 was identified as a positive marker for the clonogenic subset of cholangiocytes and was used to separate clonogenic and non-clonogenic duct cells by fluorescence-activated cell sorting. Only ST14^{hi} duct cells had the ability to generate organoids that could be serially passaged. The gene expression profiles of clonogenic and non-clonogenic duct cells were similar, but several hundred genes were differentially expressed. RNA fluorescence in situ hybridization showed that clonogenic duct cells are interspersed among regular biliary epithelium at a ~1:3 ratio. We conclude that adult murine cholangiocytes can be subdivided into two populations differing in their proliferative capacity.

INTRODUCTION

The adult liver is a highly regenerative organ that responds to injury with extensive cell proliferation. Although the mature epithelial cells (hepatocytes and cholangiocytes) can divide extensively, it has long been thought that the liver may harbor facultative stem cells which are called upon in certain chronic injury situations (Duncan et al., 2009; Miyajima et al., 2014). In the intestine, multilineage stem cells are found at the bottom of the crypts and express the R-spondin receptor LGR5 (Koo and Clevers, 2014). The adult liver of both mice and humans also harbors cells that can give rise to Lgr5$^+$ hepatic organoids comparable with those generated from the intestine (Huch et al., 2013, 2015). In the intestine, Lgr5$^+$ cells are observable during normal homeostasis and have been shown to be bona fide stem cells (Barker et al., 2007, 2010). Although adult liver does not contain Lgr5$^+$ cells during normal homeostasis, such cells can emerge under conditions of injury and can give rise to hepatic organoids *in vitro* (Huch et al., 2013). Cultured hepatic organoids display extensive self-renewal and express hepatocyte-like properties after *in vitro* differentiation. They also can produce limited *in vivo* engraftment after transplantation, but the efficiency of this process is significantly lower than with true hepatocytes.

We recently showed that the precursor to Lgr5$^+$ organoid-forming cells resides in the ductal compartments of the liver and pancreas in mice (Dorrell et al., 2014). It is currently unclear whether these highly clonogenic ductal cells are bipotential, i.e., can clonally produce both cholangiocytes and hepatocytes, in the adult liver (Espanol-Suner et al., 2012; Schaub et al., 2014; Tarlow et al., 2014a, 2014b; Yanger et al., 2013). It is also unclear whether this population contributes significantly to liver injury repair *in vivo*. Multiple genetic lineage tracing studies performed in mice argue against a contribution of ductal progenitors to the functional hepatocyte pool even with chronic injury (Grompe, 2014). Nonetheless, experiments performed in other species, most notably the rat, suggest that a bipotential liver stem cell does exist and that it resides within the cholangiocyte compartment (Evarts et al., 1989; Golding et al., 1996; Paku et al., 2001). Our previous work showed that the clonogenic (organoid-forming) population in the adult mouse liver is heterogeneous at the single-cell level (Dorrell et al., 2011, 2014) and that only approximately 1 out of 20 fluorescence-activated cell sorting (FACS)-purified biliary duct cells are clonogenic. We therefore wished to further refine the precursor population for Lgr5$^+$ hepatic organoids and determine some of their key properties, such as their transcriptome. Here we demonstrate that adult mouse biliary duct epithelium is indeed functionally and transcriptionally heterogeneous. Differential expression of the cell surface marker ST14 was used to purify and study the organoid-forming population in the adult mouse liver, defining two distinct subtypes of adult cholangiocytes.

RESULTS

Characterization of Duct Cell Heterogeneity

Biliary cells positive for the cell surface marker MIC1-1C3 have been previously shown to contain the precursors for

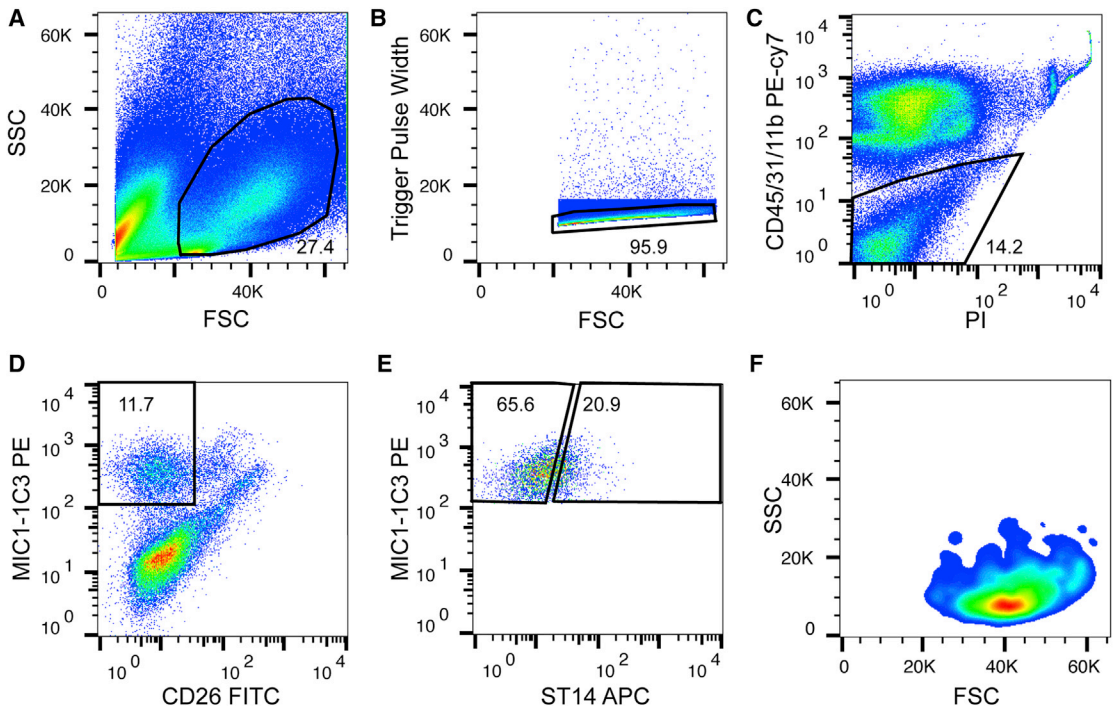

Figure 1. FACS Strategy for Adult Duct Cells

The sequence of the sorting work flow is shown from left to right in (A) to (E). Mouse liver non-parenchymal (NPC) cells were labeled with MIC1-1C3, ST14, CD26, CD31, CD45, and CD11b.

(A and B) Cells were sequentially gated based on cell size (forward scatter [FSC] versus side scatter [SSC]) (A) and singlets (FSC versus trigger pulse width) (B).

(C) Dead cells and debris were excluded by detection of propidium iodide (PI) positivity. Concurrently a combination of CD45, CD31, and CD11b antibodies was used for depleting blood, endothelium, and Kupffer cells.

(D) CD26 (DPPIV) was used for hepatocyte staining.

(E) MIC1-1C3^{+} cells can be subdivided into two populations: ST14 high (ST14^{hi}M^{+}) and ST14 low (ST14^{lo}M^{+}).

(F) Size and scatter properties of fully gated ST14^{hi}M^{+} cells.

n = 10 independent mice. See also Figure S1.

Lgr5^{+} hepatic organoids (Dorrell et al., 2014). To further enrich clonogenic cells within this fraction, we searched for cell surface markers with heterogeneous expression in this population. Analysis of the DNA microarray data of the MIC1-1C3^{+}/CD133^{+}/CD26^{-} clonogenic adult liver population (Dorrell et al., 2008, 2011) revealed several candidate markers including CD24, ANXA13, SLC34A2, COLLECTRIN, and ST14 (suppression of tumorigenicity 14). All of these were tested by FACS to determine whether they could further subdivide the clonogenic cholangiocyte population. Among the markers tested, ST14 gave the cleanest separation (Figures 1, S1E–S1G, and S1I); approximately 20.9% of cells were ST14^{hi} and 65.6% ST14^{lo}. Immunofluorescent labeling also showed that ST14 and the cholangiocyte marker EpCAM (epithelial cellular adhesion molecule) had partially overlapping distributions: EpCAM-expressing cells can be either ST14-positive or -negative (Figure S1A). Moreover, ST14 protein heterogeneity in human duct cells could also be found (Figure S4).

Robust Single-Cell-Derived Organoid-Forming Efficiency

To investigate the expansion capability of these different cholangiocyte populations, we collected MIC1-1C3^{+} cells expressing high levels of ST14 (ST14^{hi}M^{+}) and MIC1-1C3^{+} cells expressing low levels of ST14 (ST14^{lo}M^{+}) by FACS. Their clonogenic potential was then tested in a modified hepatic organoid-forming assay (Dorrell et al., 2014; Huch et al., 2013). Single ST14^{hi} and ST14^{lo} cells were deposited by FACS into a 96-well plate prefilled organoid culture medium (Figure 2A). At day 14 of culture, the ST14^{hi} cells had formed larger organoids than ST14^{lo} duct cells (Figures 2B and 2C). They also had a higher a priori organoid-forming efficiency (14 ± 4.8 organoids per 100 input cells, mean 1/7, n = 16) compared with ST14^{lo} cells (5.4 ± 2.5 organoids per 100 input cells, mean 1/22, n = 8) (Figures 2D and 2E). Large organoids (>200 μm diameter) were produced from only the ST14^{hi}M^{+} population (Figure 2F). The capacity for serial expansion was

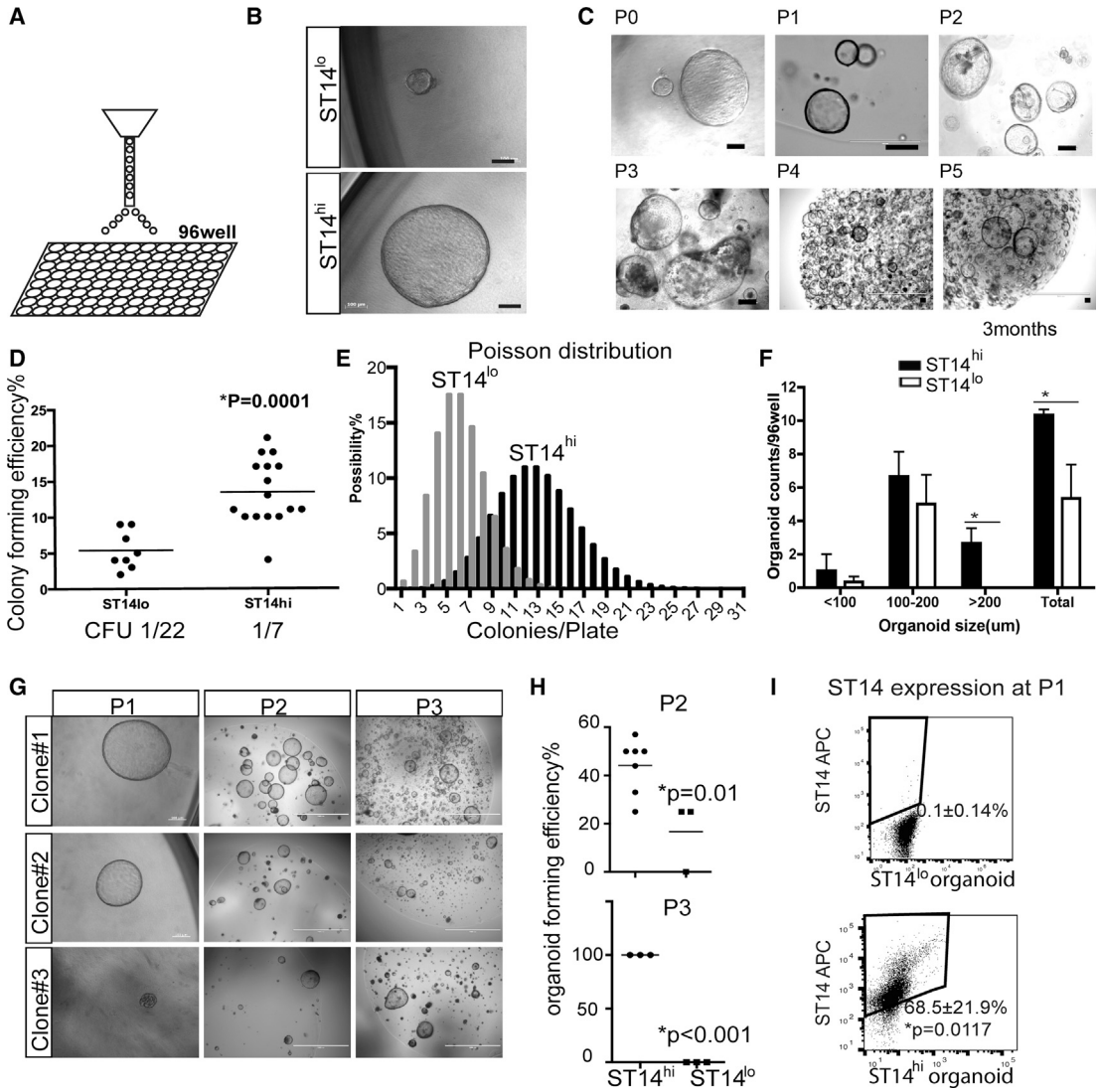

Figure 2. Clonogenicity of Biliary Duct Subsets

(A) Individual FACS-sorted ST14^{hi}M^{+}CD26^{-}CD45/31/11b^{-} and ST14^{lo}M^{+}CD26^{-} CD45/31/11b^{-} cells were directly deposited into individual cells of a 96-well plate.

(B) Representative morphology of organoids generated by M^{+}ST14^{lo} and M^{+}ST14^{hi} cells. Culture day 14. Scale bars, 100 μm.

(C) Long-term expansion of M^{+}ST14^{hi} population colonies. P, number of passages. Scale bar, 100 μm.

(D) Colony-forming efficiency of single cells. The M^{+}ST14^{lo} population had an efficiency of ~5.4% and M^{+}ST14^{hi} an efficiency of13.4%. p = 0.0001. Statistical analysis by unpaired t test. CFU, colony-forming unit (n = 8 plates from four independent mice for ST14^{lo}, n = 16 plates from eight independent mice for ST14^{hi}).

(E) Poisson distribution of M^{+}ST14^{lo} versus M^{+}ST14^{hi} organoid-forming efficiency from (D). The M^{+}ST14^{lo} population gave rise to an average of five colonies per 96-well plate while M^{+}ST14^{hi} gave rise to an average of 13. The distribution was clearly bimodal.

(F) Size distribution of organoids derived from single cells. Statistical analysis by t test (n = 3 independent experiments). *p < 0.01.

(G) Representative images of three different single-cell-derived M^{+}ST14^{hi} clones during serial passage. Scale bars, 100 μm (left panels) and 2 mm (middle and right panels).

(H) Efficiency of serial passage for the different populations. None of the organoids derived from M^{+}ST14^{lo} cells could be passaged more than three times. Statistical analysis by unpaired t test. Independent organoids for ST14^{hi} in P2, n = 7; ST14^{lo} in P3, n = 3; ST14^{hi} and ST14^{lo} in P3, n = 3.

(I) Flow-cytometry analysis of ST14 expression in the M^{+}ST14^{hi} (n = 4 independent experiments) and ST14^{lo} (n = 3 independent experiments) derived organoids after *in vitro* expansion (unpaired t test, mean ± SD, p = 0.0117).

See also Figure S2.

tested by passaging established organoids from the initial 96-well plates to 24-well plates. Organoids established from ST14^{hi} cells displayed higher proliferation rates and could be passaged more efficiently than the small organoids from ST14^{lo} cells (Figures 2G and 2H): Organoids initiated by ST14^{hi} cells could be passaged more than three times while those from ST14^{lo} cells could not be passaged more than twice (Figures 2C, 2G, and 2H). To determine whether ST14 was expressed in organoids *in vitro*, we performed FACS analysis. More than 65% of cells in the ST14^{hi} derived organoids were ST14^{+} (Figure 2I, n = 4). Moreover, we found *Lgr5* mRNA expressed only in ST14^{hi} but not ST14^{lo} cells from ST14^{hi} cell-derived organoids (Figure S3A). Furthermore, ST14^{hi} cell-derived organoids displayed low levels of expression of the mature hepatocyte marker Fah after differentiation *in vitro* (Figure S3B). Taken together, these results indicated that ST14^{hi} ductal cells had a higher colony-forming ability, grew faster, and could be serially passaged with higher efficiency than their ST14^{hi} counterparts. We therefore designated the ST14^{hi}M^{+} population as clonogenic organoid-forming biliary cells.

ST14^{hi} Cells Survive Longer Than Other Duct Cells Post Mortem

We previously reported that mouse liver harbors transplantable hepatocytes for up to 24 hr after death (Erker et al., 2010). We therefore wished to determine the post-mortem survival of organoid-forming, clonogenic biliary cells. Mice were euthanized and kept at room temperature until later cell isolation by liver perfusion. Interestingly, large numbers of viable (propidium iodide-negative) cholangiocytes could still be isolated by FACS 24 hr after death. This duct population retained clonogenic activity and was able to form organoids capable of serial passage *in vitro* (Figure S2A). Moreover, the ST14^{hi} subpopulation increased to ~45% of M^{+} duct cells compared with only 21% in the normal liver (Figure S2B). These data indicate that adult liver clonogenic cholangiocytes are resistant to prolonged warm ischemia.

ST14^{hi} Cells Are Present in Injured Liver

To assess the expression of ST14 during injury, we used the 3,5-diethoxycarbonyl-1,4-dihydrocollidine (DDC) diet and carbon tetrachloride (CCl_4) to induce liver damage as previously reported (Huch et al., 2013). Importantly, the ST14^{hi} percentage among MIC1-1C3^{+} duct cells (Figures S2C–S2F) remained stable during injury. In addition, the organoid-forming frequency of ST14^{hi} cells from the injured liver was similar to that in normal liver (Figure S2G). These findings suggest that acute liver injury did not result in a selective expansion or loss of the clonogenic cholangiocyte population.

Transcriptomes of Adult Biliary Duct Subpopulations

To compare the ST14^{hi}M^{+} and ST14^{lo}M^{+} populations at the transcriptional level, we extracted RNA from freshly FACS-sorted cells for sequencing. Multiple replicates (four ST14^{hi} and four ST14^{lo}) from independent cell isolations were analyzed. There were no significant differences between ST14^{hi} and ST14^{lo} populations in the expression of prototypical cholangiocyte cell markers such as *Sox9*, *Epcam*, and *Krt19* (Figure 3B and Table S2), confirming the biliary duct nature of both populations. However, a sizable list of genes was gene was differentially expressed between the two populations. A total of 658 genes were upregulated and 241 genes downregulated in the ST14^{hi} population using a false discovery rate (FDR) of <0.1 as the cutoff (Tables 1 and S1); 308 genes were upregulated in the ST14^{hi} population with an FDR of <0.05 and 185 genes were upregulated with an FDR of <0.01. Interestingly, ST14 itself was not differentially expressed at the mRNA level (Table S1), suggesting that the heterogeneity observable at the protein level must be due to post-transcriptional mechanisms (Brazill et al., 2000; Mahmoud et al., 2011; Zhao et al., 2015).

Gene ontogeny analysis of the differentially expressed genes showed upregulation of genes related to general stem cell properties, mammary stem cells, and hepatoblast pathways in the ST14^{hi} population. This indicates enrichment for stem/progenitor characteristics (Figure 3 and Table S3). In contrast, the cell-cycle checkpoint gene list was downregulated in the ST14^{hi} population (Figure 3D), consistent with their superior colony-forming ability and growth. Stem/progenitor cell-associated regulators such as *Wnt2b* (7.25-fold) (Flanagan et al., 2015; Goss et al., 2009; Snow et al., 2009), *Igfbp5* (10.87-fold) (Liu et al., 2015), *Bmp4* (5.60-fold) (Gouon-Evans et al., 2006), and *Gpc3* (4.45-fold) (Grozdanov et al., 2006) were more highly expressed in the ST14^{hi} population (Table 1 and Figure 3B). Interestingly, mesenchymal markers such as *Vim* (3.84-fold), the hepatic stellate cell marker *Desmin* (9.60-fold), and cell surface marker *Cd200* (2.54-fold) were enriched as well (Table 1). Lgr5^{+} cells have been shown to appear in the liver only after injury (Huch et al., 2013). Consistent with this report, *Lgr5* was not expressed in either population of ST14^{hi} cholangiocytes freshly isolated from normal liver. However, *Lgr5* gene expression was ~80-fold higher in the cultured ST14^{hi} organoids compared with the same cells in monolayer culture, while ST14^{lo} organoids did not express *Lgr5* (Figure S1H).

Anatomic Location of Clonogenic Bile Ducts

Having established that adult mouse biliary duct cells have heterogeneous organoid-forming ability, we wished to determine their anatomic location within the liver. The

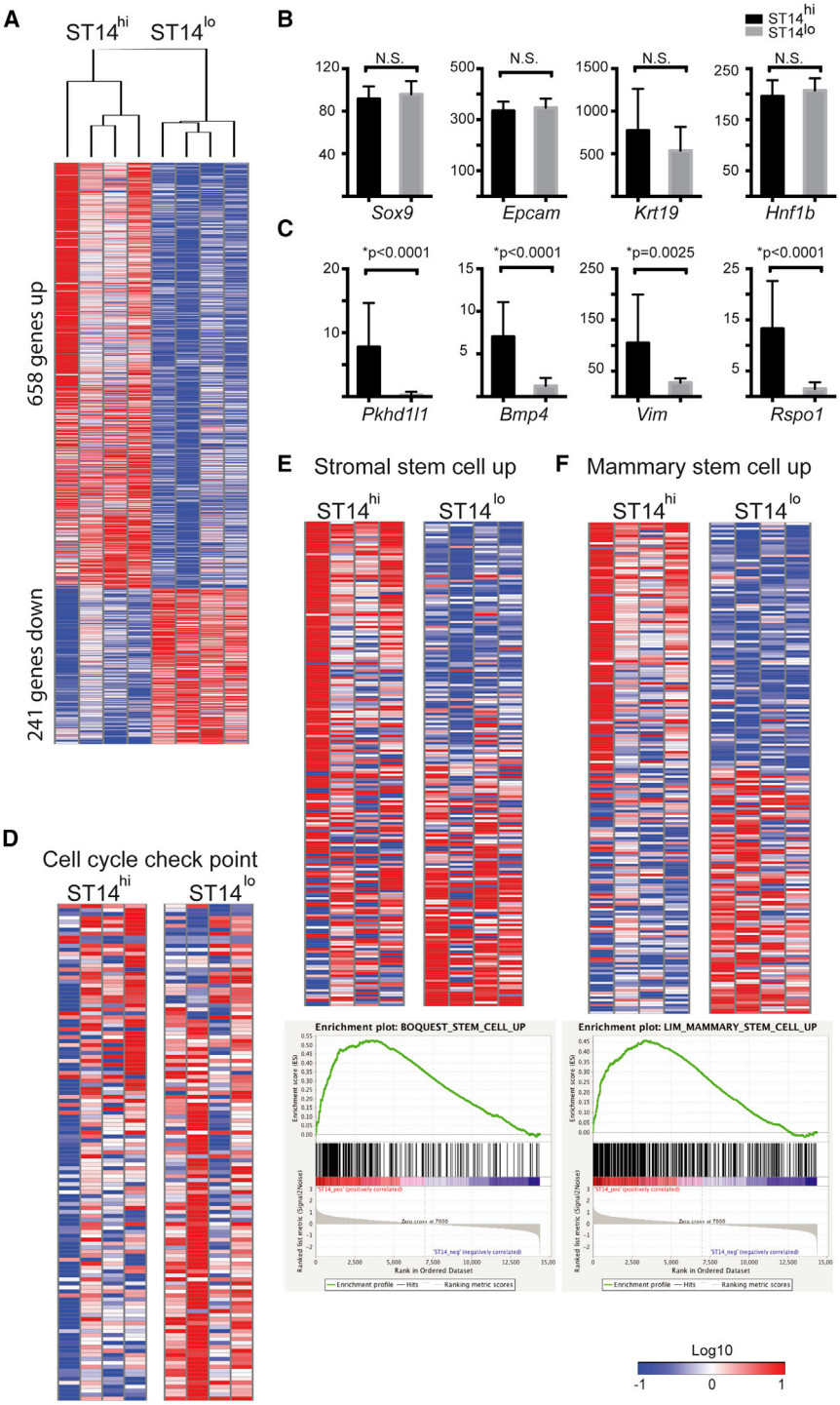

Figure 3. Transcriptome Analyses of M$^+$ST14^{hi} and M$^+$ST14^{lo} Duct Cells

(A) Kendal's tau unsupervised clustering of RNA-seq data of the M$^+$ST14^{hi} and M$^+$ST14^{lo} populations (n = 4 independent experiments for each population).

(B and C) RNA expression levels of selected individual genes. The y axis indicates RPKM (reads per kilobase per million). N.S., not significant. (B) Prototypical cholangiocyte marker expression levels were comparable in the duct populations. (C) *Pkhd1l1*, *Bmp4*, *Vim*, and *Rspo1* are examples of differentially expressed genes.

(D–F) Representation of differentially expressed gene set enrichment analysis categories. (D) Downregulated cell-cycle checkpoint genes. (E) Upregulated in stem cells (BOQUEST) (Boquest et al., 2005). (F) Upregulated in mammary stem cells (Lim et al., 2010).

RNA-sequencing (RNA-seq) data were mined for marker genes that could be used to visualize the clonogenic bile ducts by RNA fluorescence in situ hybridization (FISH). One of the genes most differentially expressed was *Pkhd1l1* (Table 1 and Figure 3B), which is highly related to the known liver disease gene *Pkhd1* (Zhang et al., 2004). The expression of this gene was 31-fold higher in ST14^{hi} cells than in ST14^{lo} cells. None of the commercially available antibodies to PKHD1L1 we tested produced clear immunofluorescent labeling. Therefore, to find the location of Pkhd1l1 expression within the cholangiocyte compartment, we performed concurrent dual-color in situ

Table 1. Selected Genes Differentially Expressed in ST14^{hi} versus ST14^{lo} Cholangiocytes

Gene		ST14^{hi} (RPKM)	FC (ST14^{hi}/ST14^{lo})	p Value	FDR
Lgals7	lectin, galactose binding, soluble 7	6	60	1.83×10^{-10}	0
Sfrp2	secreted frizzled-related protein 2	3.75	37.5	1.15×10^{-8}	0
Pkhd1l1	oolycystic kidney and hepatic disease 1-like 1	7.75	31	1.58×10^{-5}	0
Lrp2	low-density lipoprotein receptor-related protein	2.5	25	1.58×10^{-5}	0
Mrgprf	G-protein-coupled receptor MrgF	2.5	25	2.51×10^{-6}	0
Krt14	keratin 14	1.75	17.5	1.61×10^{-5}	0
Cdh11	cadherin 11	6.75	13.5	4.61×10^{-15}	0
Igfbp5	insulin-like growth factor binding protein 5	122.25	10.87	2.83×10^{-5}	0
Des	desmin	12	9.6	8.69×10^{-6}	0
Wt1	Wilms tumor 1	6.5	8.67	1.17×10^{-10}	0
Rspo1	R-spondin 1	13.25	8.25	3.61×10^{-5}	0
Cd34	CD34 antigen	16.25	8.13	1.47×10^{-5}	0
Cd248	CD248 antigen, endosialin	6	8	3.44×10^{-4}	0.01
Igfbp6	insulin-like growth factor binding protein 6	77.75	7.97	3.58×10^{-6}	0
Wnt2b	Wingless-related MMTV integration site 2b	7.25	7.25	2.75×10^{-9}	0
Ogn	osteoglycin	10.75	6.14	1.89×10^{-4}	0
Bmp4	bone morphogenetic protein 4	7	5.6	2.95×10^{-7}	0
Sulf2	sulfatase 2	5.25	5.25	2.24×10^{-6}	0
Gas1	growth arrest specific 1	21	5.25	1.83×10^{-5}	0
Gpc3	glypican 3	30	4.45	8.12×10^{-5}	0
Vim	vimentin	104.75	3.84	2.52×10^{-3}	0.056
Fgf1	fibroblast growth factor 1	10.25	3.73	6.17×10^{-7}	0
Onecut1	one cut domain, family member 1	91.25	1.8	6.02×10^{-4}	0.02
Klra2	killer cell lectin-like receptor, subfamily A	0	−15	5.74×10^{-4}	0.02
Ccl5	chemokine (C-C motif) ligand 5	0.25	−11	6.46×10^{-3}	0.1
Pla2g7	phospholipase A2, group VII	0.25	−10	2.64×10^{-3}	0.06
Clec12a	C-type lectin domain family 12, member a	0.25	−7	4.48×10^{-3}	0.08
Itgal	integrin alpha L	0.75	−5	1.69×10^{-3}	0.04
AF251705	Cd300D antigen	0.75	−4.33	1.93×10^{-4}	0
Folr2	folate receptor 2 (fetal)	2.25	−4.33	2.12×10^{-3}	0.05
Bdkrb1	bradykinin receptor, beta 1	1.25	−2.8	2.14×10^{-3}	0.05
Cybb	cytochrome b-245, beta polypeptide	2.75	−2.64	3.03×10^{-4}	0.01
Cd38	CD38 antigen	5.25	−2.0	3.32×10^{-3}	0.07

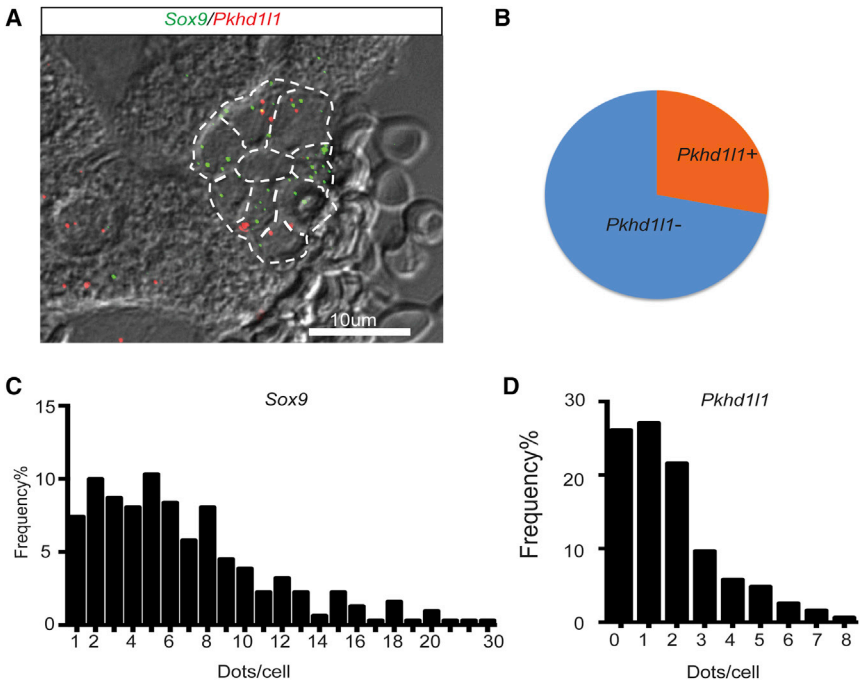

Figure 4. Clonogenic Cholangiocytes Are Interspersed within Normal Bile Ducts

(A) Representative image of *Pkhd1l1* (red) and *Sox9* (green) RNA FISH staining. Scale bar, 10 μm.

(B) Venn diagram of the *Pkhd1l1*$^{+}$ cells among all *Sox9*$^{+}$ duct cells.

(C) Frequency of *Sox9* RNA signals per duct cell.

(D) Frequency of *Pkhd1l1* RNA signals per duct cell; 60% of cells has either no or one hybridization signal, delineating the negative population.

n = 88 independent experiments from cells in four different mice. Biliary cells were identified by typical morphology in phase-contrast microscopy.

hybridization with *Pkhd1l1* and *Sox9* mRNA. Since RNA-seq revealed that *Sox9* was equally expressed in clonogenic and non-clonogenic cholangiocytes, this gene was used as a marker for both duct populations (Figure 4A). *Sox9* mRNA was found only in cholangiocytes with about seven to eight signals per cell being detected on average (Figure 4C). In contrast, *Pkhd1l1* was expressed in a subpopulation of duct cells (Figure 4D). Only ~28% of *Sox9*$^{+}$ cells were found to express *Pkhd1l1* (Figure 4B) (>1 signal/cell), which was consistent with the observed ratio of ST14^{hi} versus ST14^{lo} in MIC1-1C3^{+} cells as measured by flow cytometry (~1:3, Figure 1). These data indicate that the clonogenic subpopulation of duct cells is found within normal interlobular portal bile duct structures.

In Vivo Engraftment of Mouse Liver Organoids in FRG/N Mice

To investigate whether ST14^{hi}M^{+} mouse liver organoids could expand and repopulate damaged liver after transplantation, we dissociated organoids into single cells and performed intrasplenic transplantation of 500,000 cells (>6 passages) per recipient into Fah$^{-/-}$/Rag2$^{-/-}$/Il2rg$^{-/-}$/NOD (FRG/N) mice (n = 8 independent host mice and n = 4 organoid donor mice) as previously described (Azuma et al., 2007; Dorrell et al., 2014; Huch et al., 2013). Of these, four survived NTBC withdrawal. Ten weeks after the transplantation, liver tissues were harvested and labeled to detect hepatocyte markers FAH and HNF4A. Approximately 20 FAH-positive donor-derived hepatocytes nodules were found in each surviving mouse (Figures 5A–5D). Since the host liver does not express FAH, this observation confirms that the hepatic organoids described herein can give rise to hepatocytes and indeed represent the same Lgr5^{+} population previously reported by us (Dorrell et al., 2014; Huch et al., 2013).

DISCUSSION

Until recently there was consensus that the adult liver harbors facultative stem cells (Miyajima et al., 2014) which become activated during certain kinds of liver injury, termed oval cell injuries. These facultative liver/stem progenitor cells were deemed to be bipotential, i.e., to give rise to both cholangiocytes and hepatocytes, and be a cell with ductal phenotype located in the canal of Hering. Upon activation, liver stem cells were thought to produce proliferating duct cells (oval cells) and then differentiate into hepatocytes as they migrated out from the portal triad into the hepatic lobule. This previously well-accepted paradigm has now been challenged by lineage-tracing studies performed by several laboratories (Grompe, 2014). Consistently, these studies have shown no significant contribution of oval cells (identified as proliferating duct cells) to the hepatocyte lineage *in vivo*, at least using the standard injury models in mice.

Other recent studies, however, have demonstrated the existence of a highly proliferative cell resident in normal adult liver that can grow as an Lgr5^{+} organoid in tissue culture and give rise to hepatocytes upon transplantation,

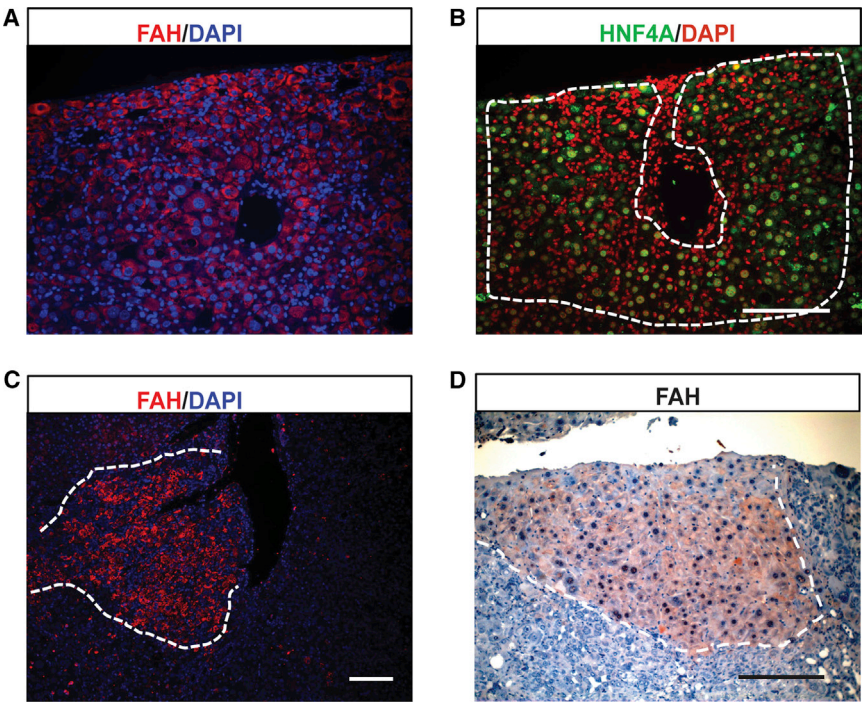

Figure 5. *In Vivo* Engraftment of ST14^{hi}-Derived Organoids

(A and B) Immunofluorescent labeling for FAH and HNF4A from serial sections (DAPI stained nuclei as blue).

(C and D) Immunofluorescent (C) and immunohistochemistry (D) staining for FAH (nuclei stained with hematoxylin) in the FRG/N mouse liver. An FAH^{+} donor-derived nodule of healthy hepatocytes is illustrated. Scale bars, 100 μm. See also Figure S4.

albeit inefficiently. Organoid-forming cells have been found to reside within the ductal compartment (Dorrell et al., 2014; Huch et al., 2015), and exist in both mice (Huch et al., 2013) and humans (Huch et al., 2015). Lineage-tracing studies demonstrated that the organoid-forming cell in adult mouse is derived from a SOX9^{+} precursor (Tarlow et al., 2014a). Although it is currently unresolved whether the SOX9^{+} adult liver progenitor can act as a hepatocyte precursor *in vivo*, these cells can be massively expanded *ex vivo*. Therefore, they could potentially serve as an abundant source of transplantable cells if their terminal differentiation into hepatocytes could be made efficient.

At most, 1 out of 20 biliary duct cells will form a primary LGR5^{+} organoid under normal conditions (Dorrell et al., 2014). This observation suggested that this population is heterogeneous and contains a subset of more highly clonogenic cells. Our experiments here clearly demonstrate that cholangiocytes in the adult mouse are indeed functionally heterogeneous and can be subdivided into clonogenic and non-clonogenic subsets. Only the organoids from ST14^{hi} cells could be serially passaged. The small primary organoids from ST14^{lo} duct cells stopped growing after two passages. Our data therefore indicate that the vast majority, if not all, of serially expandable hepatic organoids derive from the ST14^{hi} clonogenic population. The ST14^{hi} and ST14^{lo} populations were not only distinct in their organoid-forming ability but also had clear differences in gene expression. Although classic cholangiocyte genes were not differentially expressed, >10-fold differences were observed in many other transcripts. The genes most highly expressed in the clonogenic subset population are candidates to be novel markers of hepatic progenitors, as they delineate the population that produces *Lgr5*$^{+}$ liver organoids. However, it is still uncertain whether the same cells that produce hepatic organoids in culture represent bona fide stem/progenitor cells *in vivo*. Although clonogenic assays can be useful to isolate progenitors in many systems, we did not perform *in vivo* lineage tracing of the clonogenic cholangiocytes to formally prove that they are injury-induced stem/progenitor cells. Given the list of differentially expressed genes, however, it should be possible in the future to generate Cre-driver lines to specifically trace the fate of these cells *in vivo*. Interestingly, none of the many candidate stem cell genes (Table 1) has been previously considered as oval cell or progenitor markers.

Although we did not perform *in vivo* lineage tracing, we performed experiments to measure the frequency and clonogenicity of our cholangiocyte subsets during injury. Interestingly, neither the percentages nor organoid-forming abilities of the ST14$^{hi/lo}$ populations changed with injury. This could indicate that both populations regenerate equally *in vivo* despite their different clonogenic properties *in vitro*. Alternatively, the clonogenic subset may produce both ST14^{hi} and low daughters during injury. The second hypothesis is supported by the observation that single ST14^{hi} cholangiocytes can produce both ST14-high and -low offspring in organoids *in vitro*. In

contrast, ST14^{lo} cells produce only ST14^{lo} offspring *in vitro*. However, no definite conclusions can be made based on the data presented here, and lineage-tracing studies will be needed to formally evaluate the diverging possibilities.

We used one of the new subset markers, *Pkhd1l1*, to localize the clonogenic cholangiocytes in the adult liver in situ. Using RNA FISH we found that they are part of the interlobular biliary ducts in the portal triad and appear morphologically identical to regular cholangiocytes. Our analysis was conducted in only two dimensions and it was therefore not possible to clearly discern whether the *Pkhd1l1* cells were in the canal of Hering. Future detailed three-dimensional reconstructions should resolve this question.

Our data are consistent with a recent report demonstrating heterogeneity in proliferative capacity among cholangiocytes *in vivo* (Kamimoto et al., 2016). In fact the observed frequency of clonogenic duct cells and their anatomic location within the liver fit our observations well. It can be speculated that the ST14^{hi} population reported here may represent the same cells giving rise to large biliary duct clones by lineage tracing *in vivo*. However, our results also indicate differences from the model proposed by Kamimoto et al. (2016). The consistent differences in gene expression between clonogenic and non-clonogenic cholangiocytes found by us suggest inherent differences between the two populations. This is in contrast to the stochastic activation model of a homogeneous population of cholangiocytes proposed by those authors. Interestingly, the existence of distinct populations differing in growth potential has recently also been suggested for hepatocytes (Font-Burgada et al., 2015; Wang et al., 2015). It is currently unclear for both cholangiocytes and hepatocytes whether the different populations reflect different developmental lineages or whether niche signals are responsible for the divergent phenotypes.

Interestingly, we also found that organoid-forming cells were highly ischemia resistant and retained their clonogenic properties for at least 24 hr after death even at room temperature. This suggests that cadaveric tissue sources could potentially be used to establish expandable cultures of these cells, even from non-beating heart donors. This property makes liver organoids a potentially attractive source of transplantable allogeneic hepatocytes in the future, but only if their hepatocytic differentiation can be made more efficient than it is today. Indeed, the Fah transplantation studies reported here confirmed that the organoids have only rather limited hepatocytic potential. The number of FAH^{+} hepatocyte nodules per input cell was much lower than is seen with transplantation of mature hepatocytes. The development of more efficient protocols to convert expanded organoids into mature hepatocytes should be a research priority for the future.

EXPERIMENTAL PROCEDURES

Animals and Liver Cell Preparation

Eight-week-old C57B/L6 male mice were purchased from The Jackson Laboratory. All animal experimentation was conducted in accordance with protocol IS000000788 of the institutional review committee at Oregon Health and Science University. To produce single liver cell suspensions for FACS, we perfused mouse livers with 0.5 mM EGTA (Fisher) followed by collagenase (Worthington Biochemical), as described previously (Dorrell et al., 2011).

Cell Sorting and Culture

The isolation of defined non-parenchymal cell subpopulations from adult mouse liver was performed as described previously (Dorrell et al., 2011) with some modifications. In brief, cells were incubated at 4°C for 30 min with MIC1-1C3 hybridoma supernatant at a dilution of 1:20 and anti-human ST14 (Abcam) at a concentration of 1:100. For co-staining of CD133 and ST14, biotinylated anti-CD133 (eBioscience) was used. After a wash with cold PBS containing 3% fetal bovine serum, cells were labeled with phycoerythrin (PE)-conjugated donkey anti-rat and DL647-counjugated donkey anti-rabbit secondary antibodies (Jackson Immunoresearch) and allophycocyanin (APC)-Cy7-conjugated streptavidin (BD Biosciences). After another wash, the secondary antibody was blocked by a 10-min incubation in DMEM containing 5% rat serum. Cells were then incubated with fluorescein isothiocyanate-conjugated anti-CD26 (BD Biosciences) and PE-Cy7-conjugated anti-CD45 (BD Biosciences), anti-CD11b/Mac1 (BD Biosciences), and anti-CD31 (BD Biosciences) to collectively mark hematopoietic and endothelial cells for exclusion. After a final wash, cells were resuspended in holding buffer containing propidium iodide (1 μg mL^{-1}) and then analyzed and sorted with a Cytopeia influx-GS (Becton Dickinson). Flow-cytometry data were analyzed by FlowJo (Treestar). For FACS gating, isotype control stained with secondary anti-rabbit APC and anti-rat PE only were used for negative gates. Sorted populations were mixed with Matrigel (BD Bioscience) and seeded and cultured as described previously (Huch et al., 2013) with minor modifications. Culture medium consisted of Advanced DMEM/F12 (Invitrogen) supplemented with B27 and N2 (Invitrogen), 1.25 μM N-acetylcysteine (Sigma-Aldrich), SB431542, and the following growth factors: 50 ng mL^{-1} EGF (Peprotech), 10% RSPO1 conditioned medium (Huch et al., 2013), 100 ng mL^{-1} FGF10 (Peprotech), 10 mM nicotinamide (Sigma-Aldrich), and 50 ng mL^{-1} HGF (Peprotech), 100 ng mL^{-1} Noggin, and Wnt3a (R&D Systems). For the single-cell assay, cells were sorted directly into organoid medium containing 5% Matrigel in non-tissue culture-treated 96-well plates at a density of 1 cell/well. On culture day 14, organoids were trypsinized with TrypLE (Gibco) and replated into 50 μL of Matrigel droplets in a 24-well plate for further expansion. All of the antibodies are listed in Table S4.

RNA Sequencing

Cells were directly sorted and added into TRIzol-LS for RNA extraction. Libraries were made with the Illumina TruSeq protocol following the manufacturer's protocol. Four samples for each population were processed to assure robust comparisons. The sequence

reads were trimmed to 44 bases and aligned to the mouse genome NCBI37/mm9 using Bowtie (an ultrafast memory-efficient short-read aligner) version 0.12.7 (Langmead et al., 2009). We used custom scripts to count sequences in exons annotated for RefSeq mouse genes. DESeq2 (Love et al., 2014) was used to calculate the significance of differentially expressed genes based on these counts. Data were analyzed by gene set enrichment analysis (Mootha et al., 2003; Subramanian et al., 2005), and FDRs <0.25 were considered to be significant. The RNA-seq FASTQ data were submitted to the NCBI GEO.

Liver Repopulation Assay

The transplantations of ductal cell-derived organoids to Fah-deficient mice were performed as described previously (Dorrell et al., 2011; Huch et al., 2013) with some modifications. Briefly, $Fah^{-/-}Rag2^{-/-}Il2rg^{-/-}$ (FRGN) mice (Azuma et al., 2007) were pretreated with a urokinase-type plasminogen activator adenovirus 48 hr before transplantation. Before transplantation, liver organoids were exposed to a hepatocytic differentiation medium as described by Huch et al. (2015). NTBC was withdrawn from recipient animals following transplantation, and weight was monitored daily. Upon reaching 80% of their normal weight, NTBC was readministered until health was restored. After four cycles of NTBC withdrawal, mice were euthanized for immunohistochemical assessment of liver engraftment.

Immunofluorescence

Fresh mouse and human tissues were embedded in OCT compound (Sakura) and sectioned for immunofluorescence. Tissue sections were cut at 7 μm and fixed in acetone for 15 min. After washing in 0.05% PBS-Tween 20, sections were blocked at room temperature for 1 hr with 5% serum corresponding to the host species of the secondary antibody. Primary antibody was applied to tissue sections at 4°C overnight. After washing, tissue sections were stained with secondary antibodies as listed in Table S1. Tissue imaging was observed with Zeiss LSM 700 confocal microscope.

RNA Fluorescence In Situ Hybridization

Fresh frozen tissue was embedded in OCT compound and sectioned at 10 μm thickness. RNA in situ hybridization was performed using RNAscope (ACDbio) following the manufacturer's protocol. *Sox9* and *Pkhd1l1* probes were purchased from ACDbio. Tissues were imaged in a Deltavision CoreDV Widefield Deconvolution microscope. More than 300 individual duct cells from three mice were scored for signal enumeration.

RNA Isolation and qRT-PCR

Cells were FACS-sorted directly into TRI Reagent LS (MRC, catalog #TS120). RNA was extracted with isopropanol and immediately treated with DNase I (Thermo Fisher). cDNA was synthesized with the M-MLV reverse transcription kit (Thermo Fisher). Organoids were lysed into TRIzol (Thermo Fisher, #15596). Relative mRNA expression levels were assessed by qRT-PCR using the LightCycler96 real-time PCR system (Roche). Primer sequences are: mouse *Lgr5* forward 5′-AGT TAT AAC AGC TGG GTT GGC-3′, reverse 5′-GGA AGT CAT CAA GGT TAT TAT AA-3′; mouse *Gapdh* forward 5′-AAG GTC GGT GTG AAC GGA TTT GG-3′, reverse 5′-CGT TGA ATT TGC CGT GAG TGG AG-3′.

Statistical Analyses

All data are presented as mean ± SD. GraphPad Prism software was used for statistical analyses. $p < 0.05$ and $p < 0.01$ were considered to be statistically significant and highly significant, respectively.

ACCESSION NUMBERS

RNA-seq fastq files are available from the NCBI GEO under accession number GEO: GSE73897.

SUPPLEMENTAL INFORMATION

Supplemental Information includes four figures and four tables and can be found with this article online at http://dx.doi.org/10.1016/j.stemcr.2017.06.003.

AUTHOR CONTRIBUTIONS

B.L. and M.G. designed the experiments and wrote the manuscript. C.D. and P.S.C. assisted with the flow cytometry-related experiments. C.P. designed and generated the RNA-seq analysis data. A.H. assisted with the transplantation. M.F. carried out the Fah immunohistochemistry.

ACKNOWLEDGMENTS

This work was supported by NIH grants R01-DK051592 and R01 DK083355 to M.G. The authors thank OHSU core services Massively Parallel Sequencing Shared Resource, OHSU Flow Cytometry Shared Resources, Histopathology Shared Resources, and Advanced Light Microscopy core. We thank Milton Finegold and Angela Major for histology assistance. We also thank Leslie Wakefield, Devorah Goldman, Qingshuo Zhang, Yuhan Wang, and Branden Tarlow for their excellent technical assistance. M.G. is a founder and shareholder of Yecuris. OHSU has commercially licensed MIC1-1C3; authors C.D. and M.G. are inventors of this antibody. This potential conflict of interest has been reviewed and managed by OHSU.

Received: August 17, 2016
Revised: June 1, 2017
Accepted: June 1, 2017
Published: July 6, 2017

REFERENCES

Azuma, H., Paulk, N., Ranade, A., Dorrell, C., Al-Dhalimy, M., Ellis, E., Strom, S., Kay, M.A., Finegold, M., and Grompe, M. (2007). Robust expansion of human hepatocytes in $Fah^{-/-}/Rag2^{-/-}/Il2rg^{-/-}$ mice. Nat. Biotechnol. *25*, 903–910.

Barker, N., van Es, J.H., Kuipers, J., Kujala, P., van den Born, M., Cozijnsen, M., Haegebarth, A., Korving, J., Begthel, H., Peters, P.J., et al. (2007). Identification of stem cells in small intestine and colon by marker gene Lgr5. Nature *449*, 1003–1007.

Barker, N., Huch, M., Kujala, P., van de Wetering, M., Snippert, H.J., van Es, J.H., Sato, T., Stange, D.E., Begthel, H., van den Born, M.,

et al. (2010). Lgr5(+ve) stem cells drive self-renewal in the stomach and build long-lived gastric units in vitro. Cell Stem Cell *6*, 25–36.

Boquest, A.C., Shahdadfar, A., Fronsdal, K., Sigurjonsson, O., Tunheim, S.H., Collas, P., and Brinchmann, J.E. (2005). Isolation and transcription profiling of purified uncultured human stromal stem cells: alteration of gene expression after in vitro cell culture. Mol. Biol. Cell *16*, 1131–1141.

Brazill, D.T., Caprette, D.R., Myler, H.A., Hatton, R.D., Ammann, R.R., Lindsey, D.F., Brock, D.A., and Gomer, R.H. (2000). A protein containing a serine-rich domain with vesicle fusing properties mediates cell cycle-dependent cytosolic pH regulation. J. Biol. Chem. *275*, 19231–19240.

Dorrell, C., Erker, L., Lanxon-Cookson, K.M., Abraham, S.L., Victoroff, T., Ro, S., Canaday, P.S., Streeter, P.R., and Grompe, M. (2008). Surface markers for the murine oval cell response. Hepatology *48*, 1282–1291.

Dorrell, C., Erker, L., Schug, J., Kopp, J.L., Canaday, P.S., Fox, A.J., Smirnova, O., Duncan, A.W., Finegold, M.J., Sander, M., et al. (2011). Prospective isolation of a bipotential clonogenic liver progenitor cell in adult mice. Genes Dev. *25*, 1193–1203.

Dorrell, C., Tarlow, B., Wang, Y., Canaday, P.S., Haft, A., Schug, J., Streeter, P.R., Finegold, M.J., Shenje, L.T., Kaestner, K.H., et al. (2014). The organoid-initiating cells in mouse pancreas and liver are phenotypically and functionally similar. Stem Cell Res. *13*, 275–283.

Duncan, A.W., Dorrell, C., and Grompe, M. (2009). Stem cells and liver regeneration. Gastroenterology *137*, 466–481.

Erker, L., Azuma, H., Lee, A.Y., Guo, C., Orloff, S., Eaton, L., Benedetti, E., Jensen, B., Finegold, M., Willenbring, H., et al. (2010). Therapeutic liver reconstitution with murine cells isolated long after death. Gastroenterology *139*, 1019–1029.

Espanol-Suner, R., Carpentier, R., Van Hul, N., Legry, V., Achouri, Y., Cordi, S., Jacquemin, P., Lemaigre, F., and Leclercq, I.A. (2012). Liver progenitor cells yield functional hepatocytes in response to chronic liver injury in mice. Gastroenterology *143*, 1564–1575.e7.

Evarts, R.P., Nagy, P., Nakatsukasa, H., Marsden, E., and Thorgeirsson, S.S. (1989). In vivo differentiation of rat liver oval cells into hepatocytes. Cancer Res. *49*, 1541–1547.

Flanagan, D.J., Phesse, T.J., Barker, N., Schwab, R.H., Amin, N., Malaterre, J., Stange, D.E., Nowell, C.J., Currie, S.A., Saw, J.T., et al. (2015). Frizzled7 functions as a Wnt receptor in intestinal epithelial Lgr5(+) stem cells. Stem Cell Reports *4*, 759–767.

Font-Burgada, J., Shalapour, S., Ramaswamy, S., Hsueh, B., Rossell, D., Umemura, A., Taniguchi, K., Nakagawa, H., Valasek, M.A., Ye, L., et al. (2015). Hybrid periportal hepatocytes regenerate the injured liver without giving rise to cancer. Cell *162*, 766–779.

Golding, M., Sarraf, C.E., Lalani, E.N., Anilkumar, T.V., Edwards, R.J., Nagy, P., Thorgeirsson, S.S., and Alison, M.R. (1996). Oval cell differentiation into hepatocytes in the acetylaminofluorene-treated regenerating rat liver. Gastroenterology *110*, 1182–1190.

Goss, A.M., Tian, Y., Tsukiyama, T., Cohen, E.D., Zhou, D., Lu, M.M., Yamaguchi, T.P., and Morrisey, E.E. (2009). Wnt2/2b and beta-catenin signaling are necessary and sufficient to specify lung progenitors in the foregut. Dev. Cell *17*, 290–298.

Gouon-Evans, V., Boussemart, L., Gadue, P., Nierhoff, D., Koehler, C.I., Kubo, A., Shafritz, D.A., and Keller, G. (2006). BMP-4 is required for hepatic specification of mouse embryonic stem cell-derived definitive endoderm. Nat. Biotechnol. *24*, 1402–1411.

Grompe, M. (2014). Liver stem cells, where art thou? Cell Stem Cell *15*, 257–258.

Grozdanov, P.N., Yovchev, M.I., and Dabeva, M.D. (2006). The oncofetal protein glypican-3 is a novel marker of hepatic progenitor/oval cells. Lab. Invest. *86*, 1272–1284.

Huch, M., Dorrell, C., Boj, S.F., van Es, J.H., Li, V.S., van de Wetering, M., Sato, T., Hamer, K., Sasaki, N., Finegold, M.J., et al. (2013). In vitro expansion of single Lgr5+ liver stem cells induced by Wnt-driven regeneration. Nature *494*, 247–250.

Huch, M., Gehart, H., van Boxtel, R., Hamer, K., Blokzijl, F., Verstegen, M.M., Ellis, E., van Wenum, M., Fuchs, S.A., de Ligt, J., et al. (2015). Long-term culture of genome-stable bipotent stem cells from adult human liver. Cell *160*, 299–312.

Kamimoto, K., Kaneko, K., Kok, C.Y., Okada, H., Miyajima, A., and Itoh, T. (2016). Heterogeneity and stochastic growth regulation of biliary epithelial cells dictate dynamic epithelial tissue remodeling. Elife *5*. http://dx.doi.org/10.7554/eLife.15034.

Koo, B.K., and Clevers, H. (2014). Stem cells marked by the R-spondin receptor LGR5. Gastroenterology *147*, 289–302.

Langmead, B., Trapnell, C., Pop, M., and Salzberg, S.L. (2009). Ultrafast and memory-efficient alignment of short DNA sequences to the human genome. Genome Biol. *10*, R25.

Lim, E., Wu, D., Pal, B., Bouras, T., Asselin-Labat, M.L., Vaillant, F., Yagita, H., Lindeman, G.J., Smyth, G.K., and Visvader, J.E. (2010). Transcriptome analyses of mouse and human mammary cell subpopulations reveal multiple conserved genes and pathways. Breast Cancer Res. *12*, R21.

Liu, D., Wang, Y., Jia, Z., Wang, L., Wang, J., Yang, D., Song, J., Wang, S., and Fan, Z. (2015). Demethylation of IGFBP5 by histone demethylase KDM6B promotes mesenchymal stem cell-mediated periodontal tissue regeneration by enhancing osteogenic differentiation and anti-inflammation potentials. Stem Cells *33*, 2523–2536.

Love, M.I., Huber, W., and Anders, S. (2014). Moderated estimation of fold change and dispersion for RNA-seq data with DESeq2. Genome Biol. *15*, 550.

Mahmoud, L., Al-Saif, M., Amer, H.M., Sheikh, M., Almajhdi, F.N., and Khabar, K.S. (2011). Green fluorescent protein reporter system with transcriptional sequence heterogeneity for monitoring the interferon response. J. Virol. *85*, 9268–9275.

Miyajima, A., Tanaka, M., and Itoh, T. (2014). Stem/progenitor cells in liver development, homeostasis, regeneration, and reprogramming. Cell Stem Cell *14*, 561–574.

Mootha, V.K., Lindgren, C.M., Eriksson, K.F., Subramanian, A., Sihag, S., Lehar, J., Puigserver, P., Carlsson, E., Ridderstrale, M., Laurila, E., et al. (2003). PGC-1alpha-responsive genes involved in oxidative phosphorylation are coordinately downregulated in human diabetes. Nat. Genet. *34*, 267–273.

Paku, S., Schnur, J., Nagy, P., and Thorgeirsson, S.S. (2001). Origin and structural evolution of the early proliferating oval cells in rat liver. Am. J. Pathol. *158*, 1313–1323.

Schaub, J.R., Malato, Y., Gormond, C., and Willenbring, H. (2014). Evidence against a stem cell origin of new hepatocytes in a common mouse model of chronic liver injury. Cell Rep. *8*, 933–939.

Snow, G.E., Kasper, A.C., Busch, A.M., Schwarz, E., Ewings, K.E., Bee, T., Spinella, M.J., Dmitrovsky, E., and Freemantle, S.J. (2009). Wnt pathway reprogramming during human embryonal carcinoma differentiation and potential for therapeutic targeting. BMC Cancer *9*, 383.

Subramanian, A., Tamayo, P., Mootha, V.K., Mukherjee, S., Ebert, B.L., Gillette, M.A., Paulovich, A., Pomeroy, S.L., Golub, T.R., Lander, E.S., et al. (2005). Gene set enrichment analysis: a knowledge-based approach for interpreting genome-wide expression profiles. Proc. Natl. Acad. Sci. USA *102*, 15545–15550.

Tarlow, B.D., Finegold, M.J., and Grompe, M. (2014a). Clonal tracing of Sox9(+) liver progenitors in mouse oval cell injury. Hepatology *60*, 278–289.

Tarlow, B.D., Pelz, C., Naugler, W.E., Wakefield, L., Wilson, E.M., Finegold, M.J., and Grompe, M. (2014b). Bipotential adult liver progenitors are derived from chronically injured mature hepatocytes. Cell Stem Cell *15*, 605–618.

Wang, B., Zhao, L., Fish, M., Logan, C.Y., and Nusse, R. (2015). Self-renewing diploid Axin2(+) cells fuel homeostatic renewal of the liver. Nature *524*, 180–185.

Yanger, K., Zong, Y., Maggs, L.R., Shapira, S.N., Maddipati, R., Aiello, N.M., Thung, S.N., Wells, R.G., Greenbaum, L.E., and Stanger, B.Z. (2013). Robust cellular reprogramming occurs spontaneously during liver regeneration. Genes Dev. *27*, 719–724.

Zhang, M.Z., Mai, W., Li, C., Cho, S.Y., Hao, C., Moeckel, G., Zhao, R., Kim, I., Wang, J., Xiong, H., et al. (2004). PKHD1 protein encoded by the gene for autosomal recessive polycystic kidney disease associates with basal bodies and primary cilia in renal epithelial cells. Proc. Natl. Acad. Sci. USA *101*, 2311–2316.

Zhao, N., Nizzi, C.P., Anderson, S.A., Wang, J., Ueno, A., Tsukamoto, H., Eisenstein, R.S., Enns, C.A., and Zhang, A.S. (2015). Low intracellular iron increases the stability of matriptase-2. J. Biol. Chem. *290*, 4432–4446.

Stem Cell Reports, Volume *9*

Supplemental Information

Adult Mouse Liver Contains Two Distinct Populations of Cholangiocytes

Bin Li, Craig Dorrell, Pamela S. Canaday, Carl Pelz, Annelise Haft, Milton Finegold, and Markus Grompe

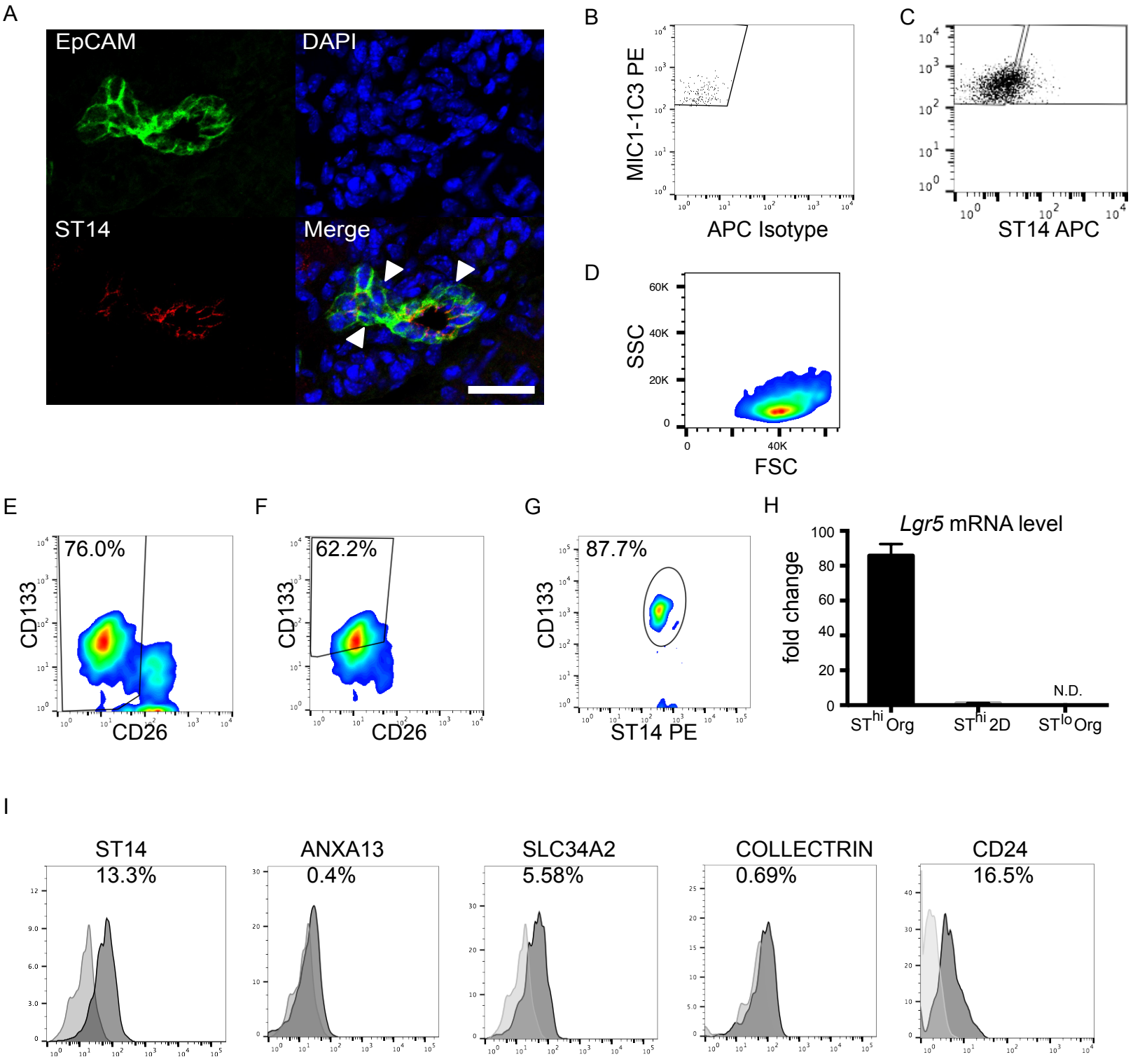

Figure S1 Related to Figure1. Evaluation of duct-subdividing antibody candidates.
(A) Representative immunohistochemistry of ST14 (red) and EpCAM (green) colocalization in mouse liver duct cells. DAPI: blue. Scale bar = 50 μm. (B-D) Flow cytometry analyses of M+26-CD45/31/11b-PI- cells stained with (B) secondary APC isotype control.only and (C) the ST14 primary antibody. (D) Size and scatter properties of fully gated ST14loM+ cells. (E-G) Flow cytometry analyses showing the extent of CD133 and ST14 coexpression in duct cells. (E) 76% of M+CD45/31/11b-PI- cells are CD26 negative. (F) in the M+CD26-CD45/31/11b-PI- cells from (E) 62.2% are CD133 expressing. (G) 87.7% of the M+ST14hi cells are CD133 positive. (H) *Lgr5* mRNA expression was activated by the organoid culture conditions in the ST14hi but not in the ST14lo organoids. (I) Antigen screening for ST14, ANXA13, SLC34A2, COLLECTRIN and CD24 in the CD26-M+ duct cells. Lighter grey delineates the isotype control.

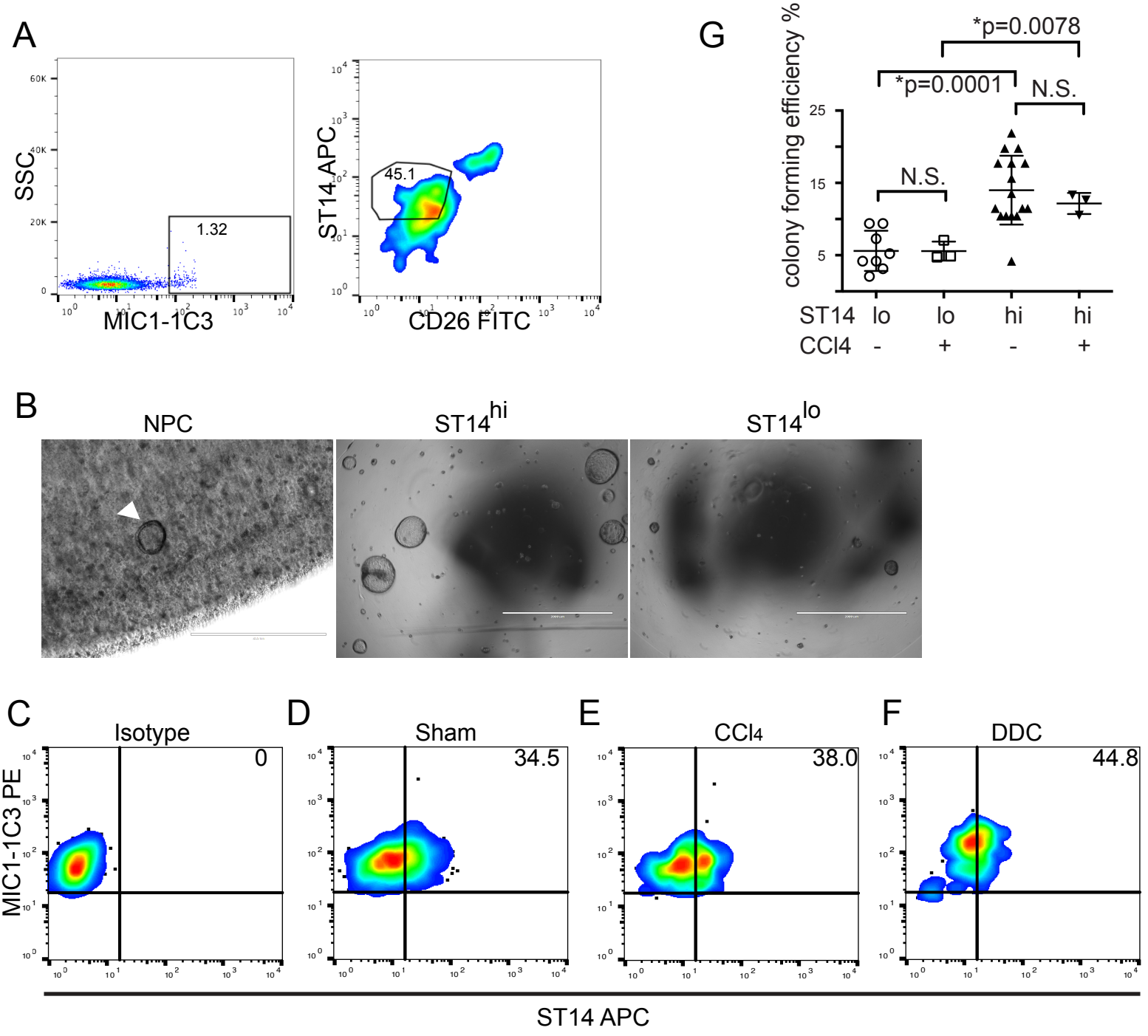

Figure S2 Related to Figure 2. Clonogenic duct cells survival during ischemia and in the injured liver
Flow cytometry analyses for MIC1-1C3+ and ST14. 45% of MIC1-1C3 duct cells were ST14hi after 24hrs of warm ischemia. After warm ischemia organoid formation was strictly limited to only ST14hi ductal cells. Far left panel: unsorted liver NPCs in organoid cell culture. FACS sorted ST14hi (middle panel) and ST14lo (far right panel) cells were embedded in Matrigel droplets at a density of 2,000 per 24 well. Culture date 14. No organoids formed from the ST14lo population. (C-G) ST14 expression in M+ liver duct cells in uninjured controls (D) and CCl4 induced liver injury day 6 (E) and DDC treated liver day 6 (F). CCl_4 was diluted in corn oil and administrated via I.P. injection at single dose of 1ml/kg body weight. Sham: corn oil only. Isotype control was used as negative gating. (G) NPCs from livers injured by CCl_4 were sorted into 96 well dishes for single cell organoid analysis. There were no significant injury-induced differences in the organoid forming ability of either population. ST14hi cells were superior to ST14lo duct cells under both conditions. Statistical analyses: Mann-Whitney U test for normal vs treated, paired t test for ST14hi vs ST14lo. Independent mice t reated with CCl_4 n=3; Independent mice treated with sham n=4.

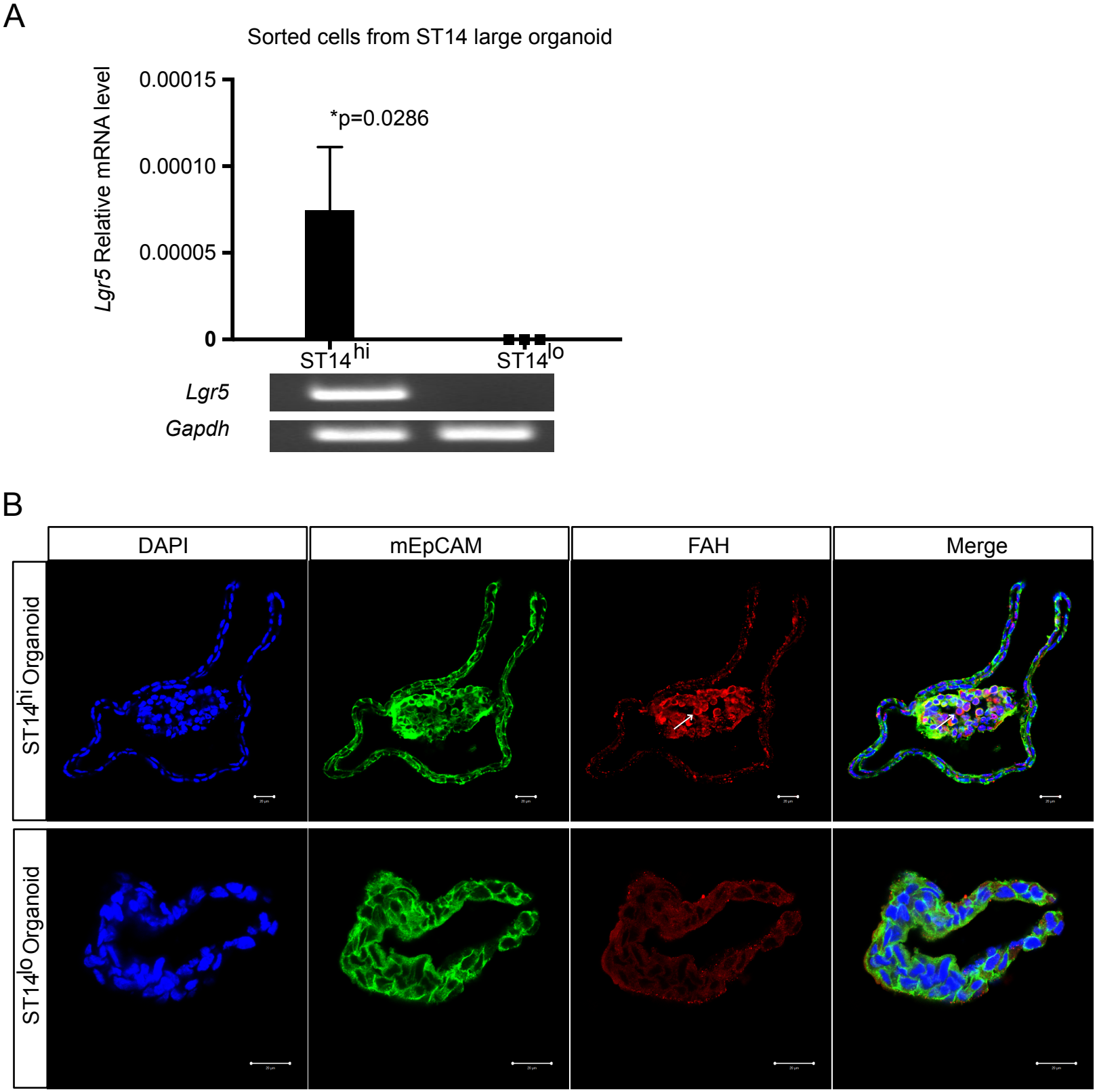

Figure S3. Related to Figure 3. Characterization of ST14hi derived organoids in vitro.
ST14hi derived organoids at passage 1 were dissociated and resorted using surface maker ST14 as in Figure 2I. (A) Relative *Lgr5* mRNA level from the ST14hi and ST14lo population detected by qPCR. Relative *Lgr5* mRNA expression was normalized to house keeping gene *Gapdh*. Single bands for the *Lgr5* and *Gapdh* PCR products were confirmed by agarose gel. Quantities were calculated with –ΔΔCt. Independent experiments n=3, upaired t test. *P=0.0286. (B) Immunofluorence staining showed Fah expression in cultured ST14hi and ST14lo derived organoids. Arrow shows FAH+ but EpCAM- cells. Scale bar = 20 μm.

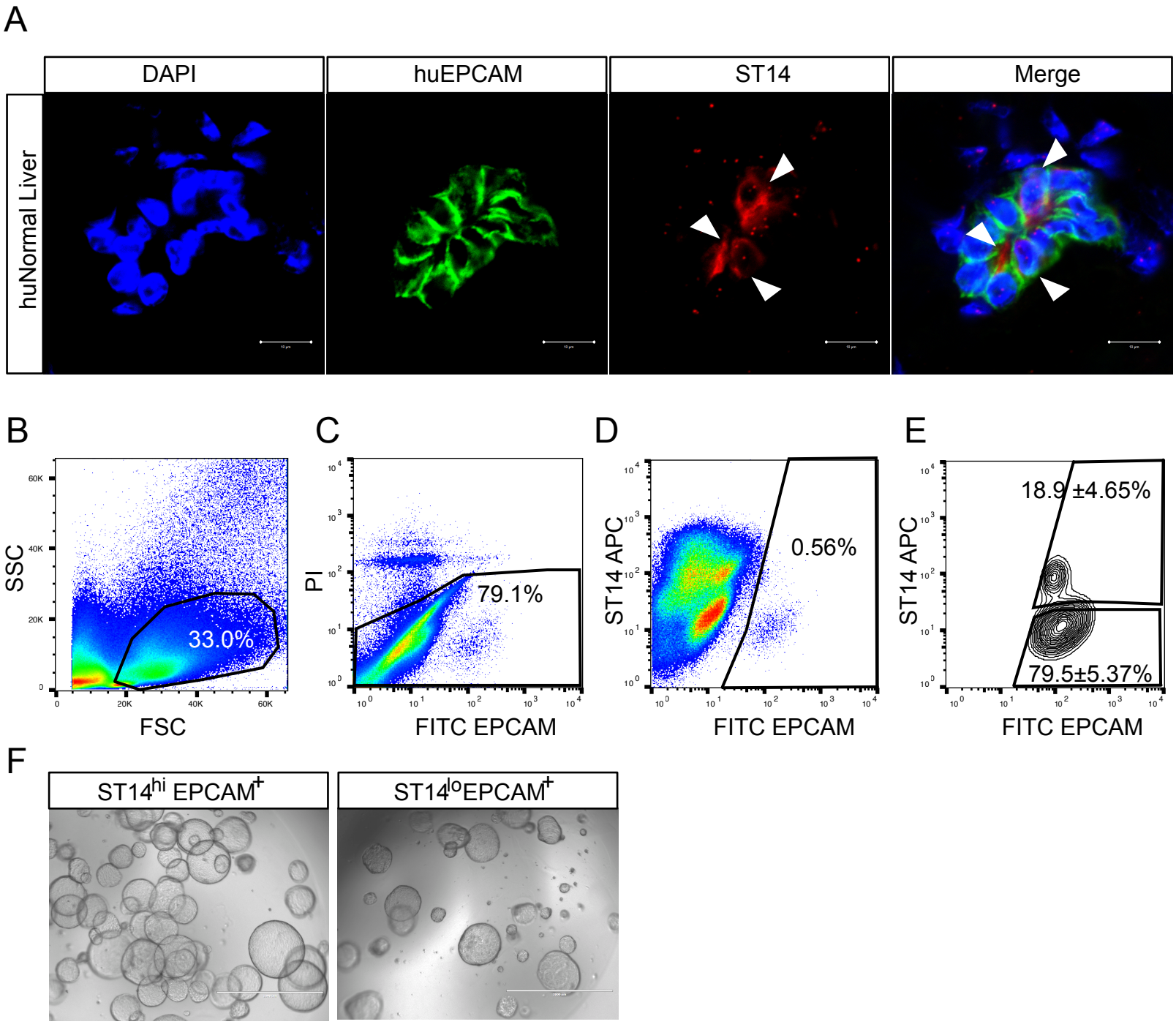

Figure S4. Related to Figure 5. ST14 protein expression in human liver.
(A) Immunofluorence showed the ST14(red) expression in the EPCAM(green) expressing duct cells in the human liver. Nuclei stained with DAPI as blue. Arrow heads show the ST14 expressing cells. Scale bar = 20 μm. (B-E) Primary human liver NPCs were FACS analyzed after staining with EPCAM and ST14. In the EPCAM+ subpopulation, 18.9±4.65% cells were ST14hi (Independent patients n=3, unpaired t test, *p=0.001) (E). (F) Sorted cells were put into matrigel organoid culture at a density of 2000 cells/well in the 24 well suspension culture plate. Scale bar = 2 mm.

Table S1 Selected hepatic biliary and progenitor markers in $ST14^{hi}$ vs $ST14^{lo}$ populations

Gene		Transcript	$ST14^{hi}$	$ST14^{lo}$	FC	Pval	FDR
St14	Suppression of tumorigenicity 14 (colon)	NM_011176	100	100	1.1	1.09	0.35
Krt19	Keratin 19	NM_008471	617.75	428.5	-1.44	0.32	0.54
Sox9	SRY (sex determining region Y)-box 9	NM_011448	114.3	119.8	-1.05	0.56	0.65
Epcam	Epithelial cell adhesion molecule	NM_008532	334.3	346.8	-1.04	0.67	0.69
Hnf1b	Transcription factor 2,transcription factor 2,	NM_009330	195.75	207.25	1.06	0.55	0.65
Cftr	Cystic fibrosis transmembrane conductance	NM_021050	16.25	20.5	1.26	0.07	0.32
Prom1	Prominin 1 (CD133 antigen)	NM_008935	181.75	187.75	1.03	0.83	0.73
Lgr5	Leucine rich repeat containing G protein coupled receptor 5	NM_010195	0.25	0	2.5	0.02	0.17
Thy1	Thymus cell antigen 1, theta	NM_009382	3	1.25	2.4	0.11	0.37
Icam1	Intercellular adhesion molecule 1	NM_010493	59.5	36.25	1.64	1	1
Bmi1	Bmi1 polycomb ring finger oncogene	NM_007552	32.75	34.75	-1.06	0.7	0.7
Cd47	CD47 antigen	NM_010581	52.25	67.5	-1.29	0.06	0.3

Tag numbers are given in RPKM for the $ST14^{hi}$ and $ST14^{lo}$ populations; FC = fold change. None of the genes listed were differentially expressed between progenitor and non-progenitor ducts.

Table S2 Selected gene sets significantly enriched in the clonogenic ST14^{hi} population

NAME	ES	NOM p-val	FDR q-val
BOQUEST_STEM_CELL_UP	0.53	0.00	0.00
ANASTASSIOU_CANCER_MESENCHYMAL_TRANSITION_SIGNATURE	0.64	0.00	0.00
LIM_MAMMARY_STEM_CELL_UP	0.46	0.00	0.00
LIEN_BREAST_CARCINOMA_METAPLASTIC	0.67	0.00	0.00
VECCHI_GASTRIC_CANCER_ADVANCED_VS_EARLY_UP	0.47	0.00	0.00
ONDER_CDH1_SIGNALING_VIA_CTNNB1	0.53	0.00	0.00
SERVITJA_ISLET_HNF1A_TARGETS_UP	0.47	0.00	0.00
MIKKELSEN_IPS_ICP_WITH_H3K4ME3_AND_H327ME3	0.50	0.00	0.00
STAMBOLSKY_TARGETS_OF_MUTATED_TP53_UP	0.56	0.00	0.01
EBAUER_TARGETS_OF_PAX3_FOXO1_FUSION_UP	0.43	0.00	0.01
ACEVEDO_LIVER_CANCER_WITH_H3K27ME3_DN	0.44	0.00	0.01
KEGG_HEDGEHOG_SIGNALING_PATHWAY	0.50	0.00	0.02
PLASARI_TGFB1_TARGETS_10HR_UP	0.38	0.00	0.02
BOQUEST_STEM_CELL_CULTURED_VS_FRESH_UP	0.35	0.00	0.02
SWEET_KRAS_TARGETS_UP	0.44	0.00	0.02
WIEDERSCHAIN_TARGETS_OF_BMI1_AND_PCGF2	0.49	0.00	0.02
DASU_IL6_SIGNALING_SCAR_UP	0.52	0.00	0.03
VERRECCHIA_RESPONSE_TO_TGFB1_C2	0.54	0.00	0.03
BOQUEST_STEM_CELL_CULTURED_VS_FRESH_DN	0.55	0.00	0.03
TURASHVILI_BREAST_DUCTAL_CARCINOMA_VS_DUCTAL_NORMAL_DN	0.39	0.00	0.03
SCHUETZ_BREAST_CANCER_DUCTAL_INVASIVE_UP	0.35	0.00	0.03
JECHLINGER_EPITHELIAL_TO_MESENCHYMAL_TRANSITION_UP	0.44	0.00	0.03
PID_HEDGEHOG_2PATHWAY	0.55	0.01	0.03
GUO_HEX_TARGETS_UP	0.43	0.00	0.04
LEE_LIVER_CANCER_HEPATOBLAST	0.62	0.01	0.04
IVANOVA_HEMATOPOIESIS_STEM_CELL_LONG_TERM	0.35	0.00	0.04
CHIANG_LIVER_CANCER_SUBCLASS_CTNNB1_DN	0.38	0.00	0.04
WHITFIELD_CELL_CYCLE_G1_S	0.37	0.00	0.06
CONRAD_STEM_CELL	0.50	0.02	0.06
SAKAI_CHRONIC_HEPATITIS_VS_LIVER_CANCER_DN	0.49	0.02	0.06
PLASARI_TGFB1_TARGETS_10HR_DN	0.33	0.00	0.08
ELVIDGE_HIF1A_AND_HIF2A_TARGETS_DN	0.37	0.00	0.08
ZHANG_GATA6_TARGETS_DN	0.39	0.01	0.09
PID_BETA_CATENIN_DEG_PATHWAY	0.54	0.05	0.09
HAN_JNK_SINGALING_DN	0.45	0.02	0.09
HOSHIDA_LIVER_CANCER_SURVIVAL_UP	0.38	0.01	0.09

Table S3 List of antibodies used

1st Antibodies

Name	IgG type	Use	Dilution	Company	Lot
ALB	Goat pAB	IF	100	Bethyl	A90-134A-6
ANXA13	Rabbit pAB	IF	100	Sigma-Aldrich	HPA019650
CD11b	Rat mAB	FACS	100	BD biosciences	552850
CD133	Biotin	FACS	100	eBioscience	13-1331-82
CD24	Rat mAB	FACS	100	BD biosciences	561079
CD31	Rat mAB	FACS	100	BD biosciences	561410
CD45	Rat mAB	FACS	100	BD biosciences	552848
CK19	Rabbit pAB	IF	500	Cell Lab Tech	A03189
COLLECTRIN	Sheep pAB	FACS	100	R&D systems	AF4965
EpCAM	Rat mAB	IF	100	BD biosciences	G8.8
EpCAM	Mouse mAB	huIF, FACS	100	DAKO	Ber-EP4
FAH	Rabbit pAB	IF	50	Grompe lab	
HNF4A	Rabbit pAB	IF	100	Santa Cruz Bio	sc-8987
MIC1-1C3	Rat mAB	FACS	20	Grompe lab	
SLC34A2	Rabbit pAB	FACS	100	Abbiotech	251343
ST14	Rabbit pAB	FACS	100	Abcam	ab28266
ST14	Rabbit pAB	huIF, FACS	100	Invitrogen	PA5-29764

2nd Antibodies

Name	IgG type	Use	Dilution	Company	Lot
Anti rat DL649	Mouse	FACS	200	JacksonImmuno	212-496-168
Anti rabbit APC	Donkey	FACS	200	JacksonImmuno	711-056-152
Anti rabbit PE	Donkey	FACS	200	JacksonImmuno	711-116-152
Anti Rat PE	Goat	FACS	200	JacksonImmuno	112-116-143
Anti rabbit Cy3	Donkey	IF	250	JacksonImmuno	711-166-152
Anti sheep AF647	Donkey	FACS	250	Jacksonimmuno	713-606-147
APC/cy7	Streptavidin	FACS	250	Biolegend	405208

Table S4 Human samples information

Use	Gender	Age	Source
IHC	Unknown	Unknown	Gift from Strom lab at University of Pittsburg, U.S.A
FACS	Female	17	Lonza, LLC. U.S.A
FACS	Male	29	Lonza, LLC. U.S.A
FACS, culture	Female	48	Lonza, LLC. U.S.A